physchem

MDPI

Article

Colloidal Synthesis and Optical Properties of Nd-Containing Mixed-Halide $CsPbBr_{3-\gamma}Cl_{\gamma}$ Quantum Dots with $\lambda_{em} \approx 458$ nm and PLQY $\approx 56\%$

Yuri K. Altudov [1], Adam M. Pshukov [1], Aneta A. Kokoeva [1], Nelli E. Pukhaeva [2,*], Ntombizonke Y. Kheswa [3] and Vasily N. Kornoukhov [1,4]

[1] Federal State Budgetary Educational Institution of Higher Education, "Kabardino-Balkarian State University Named After H.M. Berbekov", Nalchik 360004, Russia; yka@kbsu.ru (Y.K.A.); pshukov1959@mail.ru (A.M.P.); al-aneta@mail.ru (A.A.K.); kornoukhov@mail.ru (V.N.K.)
[2] Joint Institute for Nuclear Research, Dubna 141980, Russia
[3] Accelerator Research Laboratory, iThemba LABS, Somerset West 7129, South Africa; ny.kheswa@ilabs.nrf.ac.za
[4] National Research Nuclear University "Moscow Engineering Physics Institute" (NRNU MEPhI), Moscow 115409, Russia
* Correspondence: pukhaeva@jinr.ru

Abstract

This work reports the colloidal synthesis of Nd-containing mixed-halide perovskite quantum dots described as $CsPb(Nd)Br_{3-\gamma}Cl_{\gamma}$, followed by post-synthetic surface modification with an acid-activated amino-functional siloxane. This notation is used deliberately because the available FE-SEM, DLS, EDX, and optical data confirm the formation of an Nd-containing mixed-halide colloidal perovskite system, but do not provide direct crystallographic proof of substitutional Nd^{3+} incorporation at the Pb^{2+} B-site. The obtained dispersions show stable blue emission with a maximum at about 458 nm, a photoluminescence quantum yield of about 56%, an essentially invariant emission maximum when the excitation wavelength is varied from 300 to 390 nm, and monoexponential decay kinetics with a characteristic lifetime of 6.67 ± 0.97 ns. Field-emission scanning electron microscopy combined with morphometric analysis of at least 150 particles indicates a nanoscale size distribution with an average equivalent diameter of 8.8 nm, a median of 7.3 nm, and 93.25% of particles smaller than 25 nm. Dynamic light scattering confirms a narrow hydrodynamic size distribution in the 7–9 nm range and a low polydispersity index. Elemental mapping by EDX confirms the co-presence of Cs, Pb, Br, Cl, and Nd in the analyzed particles. The observed blue shift is discussed in terms of the combined effect of chloride incorporation, nanoscale size, possible Nd-related perturbation of the local electronic/defect structure, and reduced non-radiative losses after surface passivation. No definitive crystallographic assignment of Nd to a specific lattice site is claimed; the composition is therefore treated as nominal, and the structural interpretation remains provisional pending XRD/XPS or related studies.

Keywords: perovskite nanocrystals; Nd-containing systems; mixed halides; photoluminescence; surface passivation

Check for updates

Academic Editor: Aggelos Avramopoulos

Received: 12 March 2026
Revised: 20 May 2026
Accepted: 3 June 2026
Published: 16 June 2026

Copyright: © 2026 by the authors. Licensee MDPI, Basel, Switzerland. This article is an open access article distributed under the terms and conditions of the Creative Commons Attribution (CC BY) license.

1. Introduction

Blue and deep-blue emitters based on lead-halide perovskite nanocrystals are of considerable interest for display technologies, light-emitting diodes, low-threshold lasers, wavelength shifters, and exploratory radiation-detection schemes, because their emission

wavelength can be tuned over a wide range while retaining the large oscillator strength and narrow-band luminescence characteristic of direct-gap semiconductors. However, the design of efficient blue-emitting systems remains substantially more difficult than the design of green emitters. The main challenge is that the spectral shift toward shorter wavelengths is often achieved at the expense of PLQY, compositional stability, or colloidal robustness. In practical terms, the researcher must simultaneously control crystal size, halide composition, defect density, ligand chemistry, and the surrounding matrix. Recent studies on QD-in-glass composites and nanocrystal-glass systems for WLED- and photoluminescence-related applications further show that optical performance must be considered together with stability and processability [1,2]. Strategies commonly used to reach the blue region include strong quantum confinement in ultrasmall $CsPbBr_3$ QDs, growth of nanoplatelets with reduced thickness, increasing the chloride content in mixed-halide compositions, and bulk or surface passivation using heterovalent dopants and functional ligands [3–14].

Rare-earth doping is especially attractive because it can affect not only the defect chemistry of the perovskite host but also the band-edge electronic structure. In Nd-containing systems, aliovalent substitution formally introduces a cation with a different charge state and a different ionic radius compared with Pb^{2+}. This may alter local coordination, require charge compensation, and thereby change the balance between radiative and non-radiative recombination pathways. At the same time, the benefits of rare-earth incorporation are highly sensitive to the real mode of incorporation, to dopant concentration, and to the surrounding surface chemistry. Literature reports indicate that moderate Nd^{3+} concentrations can improve stability and sometimes enhance luminescence relative to undoped analogues, whereas excessively high nominal contents can increase structural disorder and introduce parasitic relaxation channels [6,9–14]. This makes the study of high-Nd nominal compositions scientifically relevant even when the exact crystallographic position of the dopant is not yet proven.

A particularly relevant reference point for the present work is the study by Chiba et al. [15], who demonstrated $NdCl_3$-treated $CsPbBr_3$ perovskite nanocrystals for blue light-emitting devices. In that work, the authors used post-synthetic room-temperature treatment with $NdCl_3$ and observed simultaneous Nd and Cl signals by XPS, blue emission at 478 nm, and a very high PLQY of 97% in solution. Importantly, their data also indicated that Nd was probably located mainly at or near the nanocrystal surface rather than being unambiguously incorporated as a bulk B-site substituent. This observation is directly relevant to the interpretation of Nd-containing mixed-halide perovskite nanocrystals and supports a cautious description of the present material as $CsPb(Nd)Br_{3-\gamma}Cl_\gamma$ rather than as a structurally proven $CsPb_{1-x}Nd_xBr_{3-\gamma}Cl_\gamma$ solid solution.

A second important design variable is halide composition. Partial replacement of Br^- by Cl^- is a straightforward route to increase the effective band gap and push the emission into the blue spectral region. Nevertheless, chloride-rich systems frequently suffer from lower photoluminescence efficiency, increased susceptibility to compositional relaxation, and stronger sensitivity to surface defects. Therefore, an efficient blue emitter must be evaluated not only by the position of the emission maximum but also by the stability of that maximum under different excitation conditions, the luminescence decay kinetics, the size distribution of the particles in dispersion, and the quality of the surface passivation layer. For colloidal applications, including luminescent liquid matrices and solution-processed photonic systems, dispersibility and resistance to aggregation are as important as the absolute value of PLQY.

In our earlier work on Nd-containing perovskite quantum dots, we demonstrated that hot-injection synthesis can produce blue-shifted emission in Nd-containing lead-halide systems, but the description of the experimental protocol and the discussion of the results

were relatively concise [16]. The present study extends that direction in three ways. First, it describes a larger-scale synthetic route performed in a 2 L reactor, which is relevant from the standpoint of reproducibility and scale-up. Second, it uses a mixed-halide formulation with the nominal composition $CsPb(Nd)Br_{3-\gamma}Cl_{\gamma}$ together with post-synthetic surface modification by acid-activated APDMS, and it examines the resulting spectral, kinetic, and morphometric characteristics in greater detail. Third, it compares the resulting material with selected recent examples of blue-emitting perovskite nanomaterials and explicitly discusses the limitations of the available dataset. The aim of the work is therefore not to claim definitive structural proof of Nd incorporation, but to present a reproducible colloidal route that yields blue emission around 458 nm with moderate PLQY and to analyze why this balance of properties may be technologically interesting.

2. Materials and Methods

2.1. Materials and Equipment

Reagents. The following reagents were used as received, without additional purification: cesium carbonate (99.99%, Sigma-Aldrich, 3050 Spruce Street, St. Louis, MO 63103, USA), lead bromide (99.999%, Sigma-Aldrich, 3050 Spruce Street, St. Louis, MO 63103, USA), lead chloride (99.999%, Sigma-Aldrich, 3050 Spruce Street, St. Louis, MO 63103, USA), neodymium chloride hexahydrate (99.9%, Alfa Aesar, Ward Hill, MA, USA), oleic acid (OA, 90%, Sigma-Aldrich, 3050 Spruce Street, St. Louis, MO 63103, USA), oleylamine (OLA, 80–90%, Acros Organics, Geel, Belgium), xylene (99.8%, HPLC grade, Fisher Chemical, Fair Lawn, NJ, USA), 1-octadecene (ODE, 90%, Fluka, Buchs, Switzerland), acetone (analytical grade, Khimmed, Moscow, Russia), bis(aminopropyl)-polydimethylsiloxane (Mw 27000, APDMS, Sigma-Aldrich, 3050 Spruce Street, St. Louis, MO 63103, USA), hydrochloric acid (reagent grade, Khimmed, Moscow, Russia), and propyl acetate (reagent grade, Vekton, St. Petersburg, Russia). The choice of OA and OLA corresponds to a standard ligand environment for lead-halide perovskite nanocrystals, while APDMS was used as a post-synthetic modifier to improve surface passivation and colloidal stability.

Instrumentation. Morphology was studied by field-emission scanning electron microscopy using a TESCAN MAIA 3 microscope (TESCAN GROUP, a.s., Libušina třída 863/21, 623 00 Brno, Czech Republic). Elemental analysis and spatial distribution of the main elements were assessed by EDX mapping in the same microscopy workflow. It should be emphasized that EDX was used to confirm elemental co-presence and microscale distribution, not to prove lattice substitution or phase purity. Steady-state excitation and emission spectra were recorded on a PerkinElmer LS 55 luminescence spectrophotometer (PerkinElmer, Waltham, MA, USA) controlled by FL WinLab software. A 2D excitation–emission dataset was acquired to evaluate the stability of the emission maximum with respect to excitation wavelength. The PLQY was measured using an integrating sphere configuration. Time-resolved photoluminescence decay kinetics were recorded and fitted with a monoexponential model. Hydrodynamic sizes were obtained by dynamic light scattering on a Malvern Zetasizer Nano Series instrument (Malvern Panalytical Ltd., Enigma Business Park, Grovewood Road, Malvern, Worcestershire WR14 1XZ, UK). Unless explicitly indicated otherwise, all measurements were performed at room temperature in the range 18–25 °C.

2.2. Synthesis of Perovskite Nanoparticles

Preparation of cesium oleate precursor. Cesium oleate was prepared by dissolving 1.084 g of cesium carbonate in a mixture of 4 mL of oleic acid and 40 mL of 1-octadecene. The mixture was held at 120 °C under vacuum until a clear, homogeneous solution was obtained. This treatment removes volatile impurities and moisture and promotes the

conversion of cesium carbonate into a reactive cesium oleate precursor suitable for rapid injection. The precursor was kept warm to avoid crystallization and viscosity-related injection artifacts.

Preparation of the surface modifier. The post-synthetic passivating formulation was prepared by adding 50 µL of hydrochloric acid to 5 g of APDMS in 10 mL of xylene. The mixture was subsequently evaporated under vacuum and rediluted with xylene to a final volume of 10 mL. In practical terms, this procedure generates an acid-activated amino-functional siloxane environment that can interact with undercoordinated surface sites of the nanocrystals and improve the surface chemical shell after synthesis and purification.

Synthesis of perovskite nanoparticles. In contrast to our earlier smaller-scale procedure [9], the synthesis was carried out in a 2 L three-neck flask. First, 70 mL of oleylamine and 50 mL of oleic acid were placed in the flask and degassed under vacuum at 120 °C. Degassing at this stage is important because residual moisture and oxygen strongly affect lead-halide precursor solubility and can introduce uncontrolled defects into the final product. After degassing, 0.875 g of neodymium chloride, 3.6 g of lead bromide, and 0.3 g of lead chloride were added to the ligand mixture. The salt mixture was dissolved under vacuum at 120 °C until a visually homogeneous precursor solution was obtained. The solution was then diluted with 700 mL of ODE and heated under argon flow to 165 °C. Once the target temperature had stabilized, 25 mL of the warm cesium oleate precursor was rapidly injected into the reaction mixture. The reaction was intentionally kept very short: after 5 s, the heating mantle was removed and 400 mL of cold xylene at about −10 °C was added to quench crystal growth. Such a short growth period is consistent with the goal of maintaining particles in the strongly nanoscale regime and avoiding broadening of the size distribution. After complete cooling, the crude product was diluted 1:1 with propyl acetate and centrifuged for 5 min at 8000 rpm to isolate the perovskite fraction. The resulting precipitate was dispersed in 90 mL of xylene, after which 10 mL of the APDMS-based surface modifier was added under vigorous stirring. The modified quantum dots were reprecipitated with a threefold excess of acetone, separated, and finally dispersed in 100 mL of xylene. Large aggregates were removed by a final centrifugation step for 1 min at 4000 rpm. The purified dispersion was used for optical and size-distribution measurements.

2.3. Measurement Methods

Dynamic light scattering. Particle size measurements were performed on a Malvern Zetasizer Nano Series analyzer (Malvern Panalytical Ltd., Enigma Business Park, Grovewood Road, Malvern, Worcestershire WR14 1XZ, UK) at 25 °C using quartz cuvettes. The instrument records the autocorrelation function of temporal fluctuations of the scattered laser intensity, from which the translational diffusion coefficient is obtained. Hydrodynamic diameter values were then calculated using the Stokes–Einstein relation. In addition to the size distribution, the instrument provided Z-average values and estimates of the polydispersity index (PDI), as well as number-, intensity-, and volume-weighted distributions. DLS was used here not as a substitute for direct microscopy but as a complementary characterization tool to verify that the purified dispersions employed in the optical experiments did not exhibit strong aggregation.

Spectroscopy, microscopy, and data treatment. FE-SEM morphology and EDX mapping were carried out using a field-emission instrument; morphometric analysis of the FE-SEM images was performed using segmentation procedures applied to at least 150 particles. Steady-state optical spectra were acquired on a PerkinElmer LS 55 spectrophotometer. A 2D excitation–emission map was constructed on an excitation grid covering 300–390 nm in order to test whether changes in excitation energy shifted the position of the emission maximum. PLQY was measured with an integrating sphere. Time-resolved

photoluminescence decay kinetics were approximated by a monoexponential function of the form $I(t) = A \exp(-t/\tau) + C$, where A is amplitude, τ is the characteristic decay time, and C is the background term. This model was chosen because it provides an adequate first-order description of the observed decay in the present samples.

Experimental reproducibility and scope of inference. The present work is focused on the physicochemical characterization of the obtained blue-emitting dispersion rather than on a broad combinatorial optimization campaign. Accordingly, the reported values should be interpreted as characteristic parameters of the synthesized material under the stated preparation and purification conditions. The nominal precursor composition is used throughout the manuscript because the currently available dataset does not include crystallographic proof of the exact Nd lattice position or a full quantitative elemental balance at the single-particle level. Nevertheless, the combination of EDX mapping, stable blue emission, narrow DLS distribution, and monoexponential decay provides a self-consistent dataset for discussing the optical behavior of the resulting colloidal system.

3. Results and Discussion

3.1. Composition, Morphology and Mapping of Elements

Throughout this work, the composition of the obtained material is described as Nd-containing mixed-halide $CsPbBr_{3-\gamma}Cl_{\gamma}$ quantum dots, or more compactly as $CsPb(Nd)Br_{3-\gamma}Cl_{\gamma}$. This notation reflects the experimental evidence more accurately than the formula $CsPb_{0.8}Nd_{0.2}BrCl_2$, because Pb^{2+} and Nd^{3+} have different charge states and the present dataset does not prove a simple substitutional solid solution of the type $CsPb_{1-x}Nd_xX_3$. The precursor mixture contained a high nominal amount of Nd, but SEM/EDX mapping confirms only the presence and spatial association of Nd with the particle ensemble. It does not establish the crystallographic position of Nd or exclude surface-bound Nd species and highly dispersed secondary Nd-containing phases below the detection limit of the employed methods.

Therefore, the term $CsPb(Nd)Br_{3-\gamma}Cl_{\gamma}$ is used as a chemically cautious notation indicating an Nd-containing mixed-halide perovskite quantum-dot system. Additional XRD, XPS, HR-TEM, or X-ray absorption studies would be required to determine whether Nd is incorporated into the lattice, located at the surface, or present in another highly dispersed chemical environment. The corresponding FE-SEM image is shown in Figure 1.

Energy-dispersive X-ray spectroscopy (EDX) mapping for Cs, Pb, Br, Cl, and Nd confirms that all principal elements associated with the nominal formulation are present in the analyzed regions. The spatial distribution of the signals does not indicate macroscopic segregation of the Nd-containing component, which supports the statement that neodymium is associated with the particle ensemble rather than present only as a separate micron-scale phase. At the same time, EDX mapping cannot establish the crystallographic location of Nd and cannot distinguish between true lattice incorporation, surface-associated Nd species, and highly dispersed secondary phases below the detection limit of the present approach. Therefore, the compositional discussion in this article is intentionally framed in terms of nominal composition and observed elemental co-localization. The corresponding elemental maps are shown in Figure 2.

The observed minor local aggregation is attributed mainly to the precipitation and drying steps from xylene during sample preparation for microscopy. This interpretation is consistent with the fact that the optical and DLS measurements, which were carried out in liquid dispersions, do not show evidence of strong polydispersity or large aggregated fractions dominating the signal.

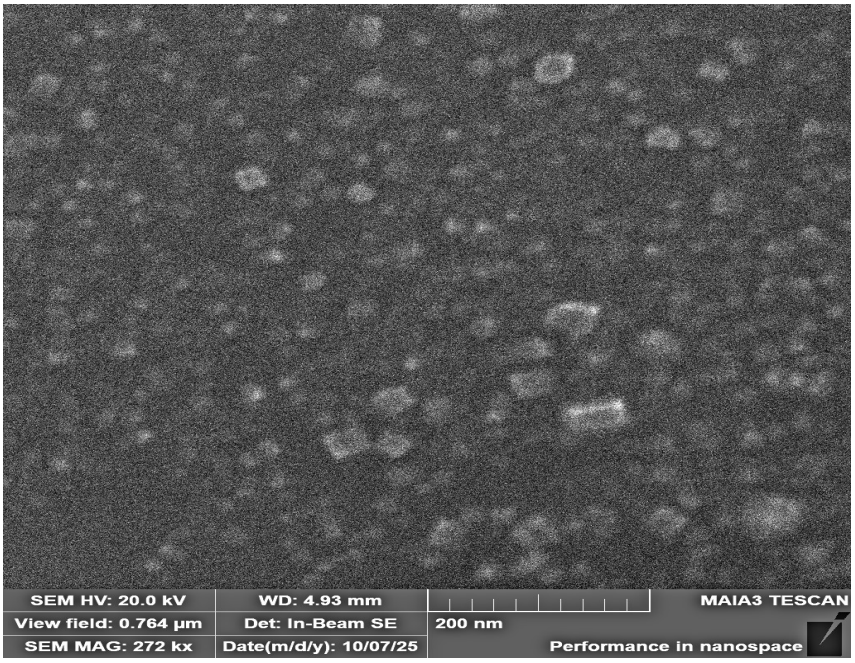


Figure 1. SEM image of CsPb(Nd)$Br_{3-\gamma}Cl_{\gamma}$ quantum dots (scale bar: 200 nm). The particle morphology is polycrystalline, and the sizes are ≈8–9 nm, consistent with DLS.

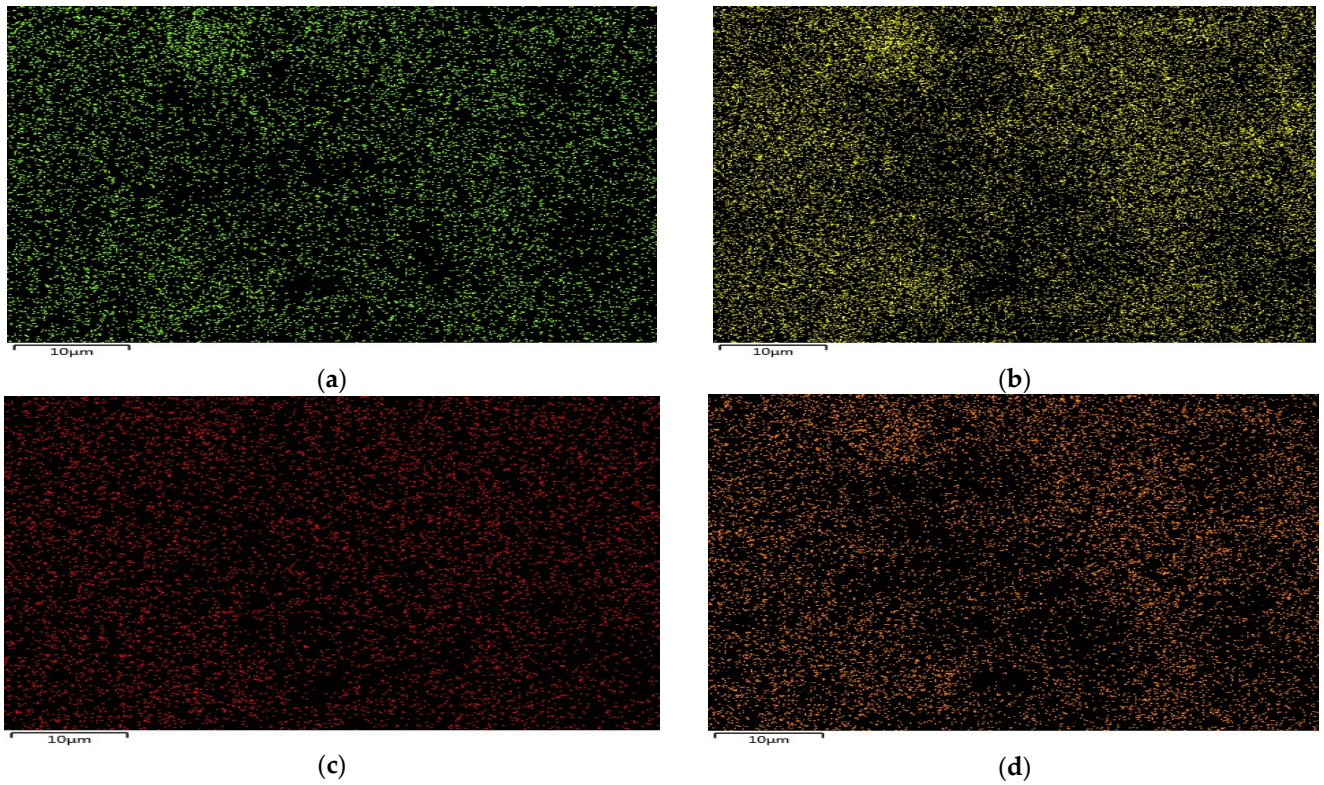


Figure 2. EDX mapping of elements in nanocrystals: (**a**) Br, (**b**) Cs, (**c**) Nd, and (**d**) Pb. The maps confirm the co-presence and spatial distribution of the corresponding elements in the analyzed regions; they should not be interpreted as proof of crystallographic Nd substitution or complete phase purity.

Dynamic light scattering further supports the conclusion that the purified dispersions used for optical measurements are stable on the colloidal level. The hydrodynamic size distribution is close to Gaussian, with the principal maximum in the 7–9 nm range, a

Z-average of approximately 8–9 nm, and a low polydispersity index of about 0.1–0.2. The agreement between DLS and FE-SEM is important because these methods probe different aspects of the material: SEM measures projected particle dimensions in the dry state, whereas DLS reflects the hydrodynamic size of the dispersed objects together with their ligand shell and solvation environment. Their mutual consistency indicates that severe aggregation is absent and that the particles remain well dispersed after purification and surface modification. The corresponding DLS size distribution is shown in Figure 3.

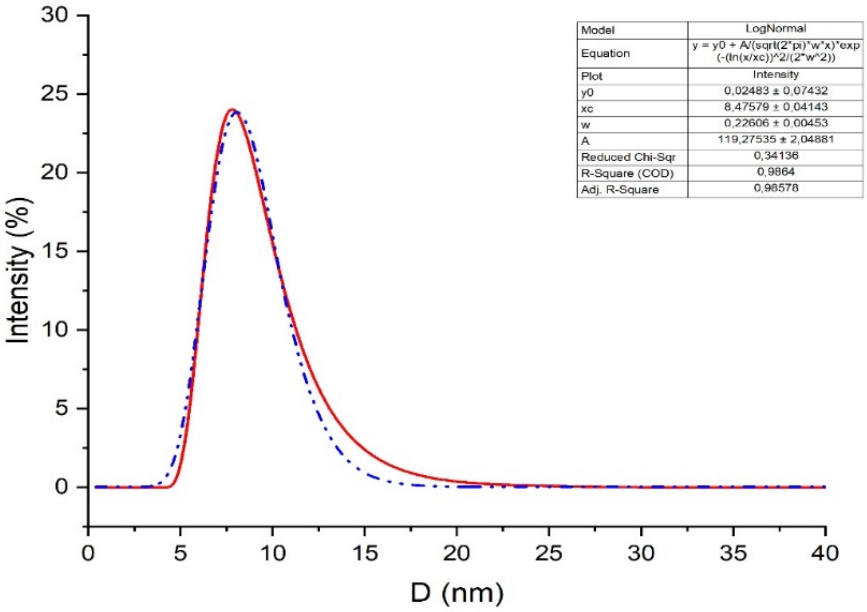


Figure 3. Quantum dot size distribution based on DLS data. The blue dashed line corresponds to the experimental DLS distribution measured at 25 °C, and the red solid line corresponds to a lognormal fit. The Gaussian-like maximum is at ~8 nm (Z-average ≈ 8.8 nm, PDI ≈ 0.1), confirming the low degree of aggregation and narrow size distribution.

3.2. Stationary Optics: Excitation–Emission

Taken together, the FE-SEM, EDX, and DLS results show that the synthesis protocol produces a chemically heterogeneous but physically well-defined colloidal system at the nanoscale. This is an essential prerequisite for meaningful interpretation of the optical data, because broad particle-size distributions or uncontrolled aggregation would obscure the origin of the observed emission behavior.

The steady-state optical response of the synthesized material is characterized by an excitation maximum near 350 nm and a broad emission band centered in the 450–460 nm region, typically at about 458 nm. The position of the emission maximum remains essentially unchanged when the excitation wavelength is varied over the 300–390 nm interval. Such excitation-independent emission behavior indicates that the dominant observed radiative response is associated with a relatively stable ensemble of emissive states under the present measurement conditions. However, this observation alone does not exclude minor contributions from surface or defect-related states. The corresponding excitation–emission contour map is shown in Figure 4.

The contour excitation–emission plot shown in Figure 4 and the 3D excitation–emission surface shown in Figure 5 shown in Figures 4 and 5 provide a compact visualization of this behavior. The main emission ridge remains located near 458 nm across the accessible excitation range, while secondary features are weak. This spectral invariance is relevant for two reasons. First, it suggests a degree of electronic uniformity in the emitting ensemble despite the complexity of the nominal mixed-halide and Nd-containing composition. Sec-

ond, it is advantageous for applications requiring stable color coordinates or a predictable wavelength-shifting response under different excitation conditions. In practice, a fixed emission maximum simplifies subsequent coupling of the nanocrystals to photodetectors, optical filters, or liquid host matrices. The blue position of the emission maximum should be viewed in the broader context of lead-halide perovskite nanocrystal photophysics. Undoped bromide-rich CsPbBr3 QDs typically emit in the green region, whereas a shift toward approximately 458 nm requires a substantial change in particle size, halide composition, defect chemistry, or their combination. In the present system, the spectral position is therefore consistent with the combined influence of chloride incorporation, nanoscale size, and possible Nd-related modification of the host lattice or surface chemistry.

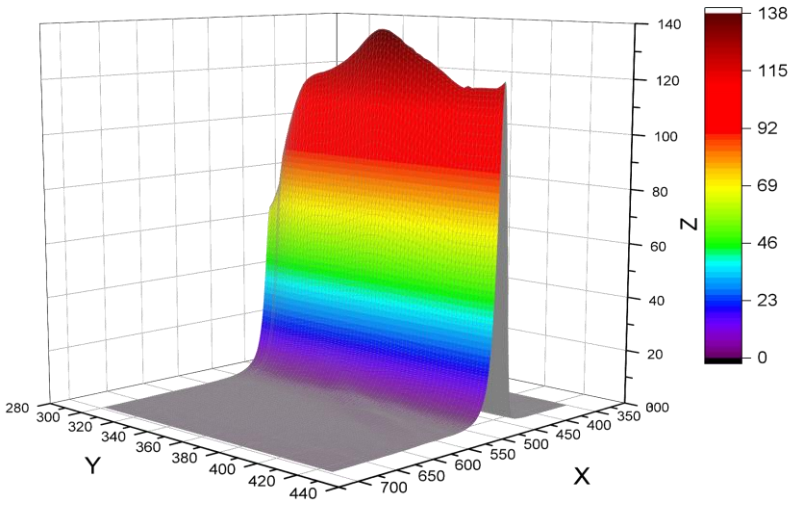


Figure 4. Photoluminescence contour map ("excitation–emission") of CsPb(Nd)$Br_{3-\gamma}Cl_{\gamma}$ nanocrystals. x-axis: emission wavelength (400–700 nm); y-axis: excitation wavelength (300–430 nm). It is evident that the maximum intensity (yellow color) occurs at ~458 nm, regardless of the excitation wavelength in the range of 300–390 nm.

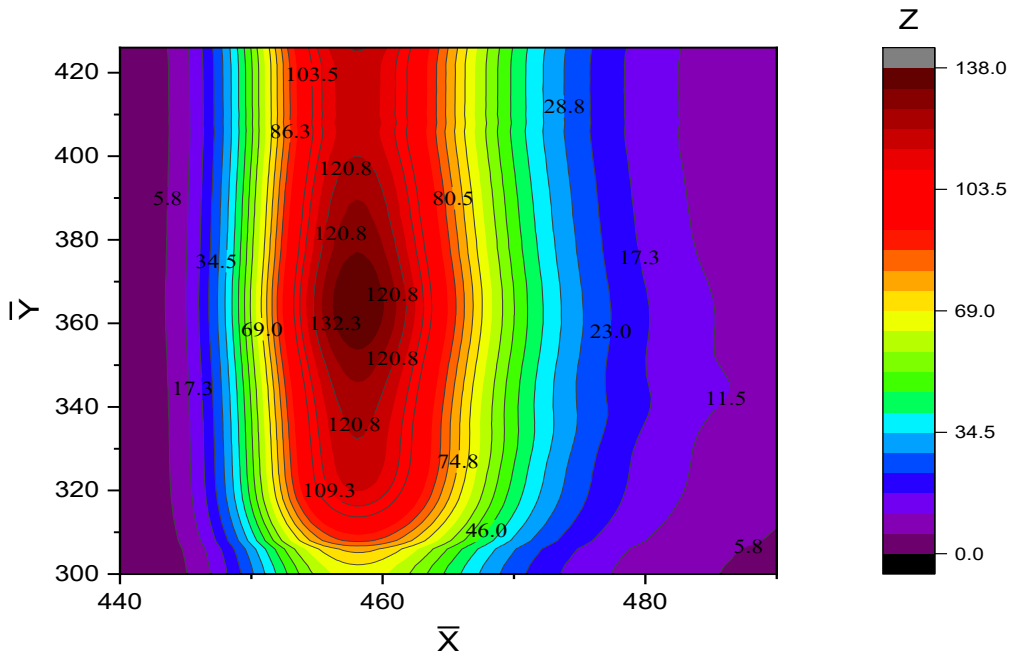


Figure 5. Three-dimensional surface of the photoluminescence spectrum of the same CsPb(Nd)$Br_{3-\gamma}Cl_{\gamma}$ nanocrystals. X-axis: λ_{em}; Y-axis: λ_{exc}; Z-axis: normalized emission intensity. The horizontal emission ridge at ~458 nm does not shift noticeably with changing excitation wavelength, indicating a stable dominant emission channel under the applied measurement conditions.

The integrated photoluminescence quantum yield of the synthesized quantum dots is about 56%, which is a notable value for a blue-emitting Nd-containing mixed-halide system. The decay kinetics of time-resolved photoluminescence are well approximated by a monoexponential function, $I(t) = A \exp(-t/\tau) + C$, with $\tau = 6.67 \pm 0.97$ ns, $A = 0.247 \pm 0.013$, and $C = -0.0189 \pm 0.009$. A monoexponential decay does not by itself prove that only one microscopic emissive channel exists; however, it does indicate that under the present measurement conditions one characteristic relaxation time dominates the luminescence response. The corresponding decay curve is shown in Figure 6.

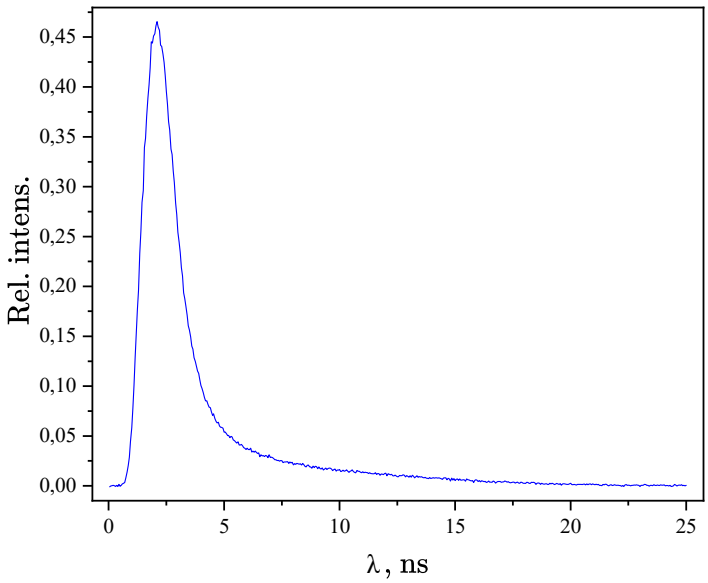


Figure 6. Time-resolved photoluminescence decay kinetics. The x-axis shows time t in ns, and the y-axis shows relative photoluminescence intensity.

3.3. Quantum Yield and Decay Dynamics

The observed lifetime is consistent with efficient radiative recombination in a colloidal perovskite ensemble where strong trapping is at least partially suppressed. In blue-emitting systems, this point is particularly important because aggressive band-gap engineering often increases the density of non-radiative pathways. The simultaneous observation of blue emission, moderate-to-high PLQY, and a short characteristic lifetime therefore suggests that the APDMS-assisted surface treatment is beneficial and that the dominant emissive states are not heavily quenched by surface traps. At the same time, the absence of a direct comparison with an untreated control sample means that the quantitative contribution of the post-synthetic modification cannot yet be isolated rigorously.

3.4. Mechanism of the Blue Shift and the Possible Role of Nd/Cl

The blue emission observed for the present $CsPb(Nd)Br_{3-\gamma}Cl_{\gamma}$ quantum dots should be interpreted as the result of several concurrent factors rather than as direct proof of Nd^{3+} substitution at the Pb^{2+} site. The first and most straightforward factor is partial replacement of Br^{-} by Cl^{-}, which increases the effective band gap of the perovskite host and shifts the emission toward shorter wavelengths. The second factor is the nanoscale size of the particles, which can contribute to additional spectral shifting through quantum-confinement effects. The third factor is the presence of Nd-containing species, which may modify the local electronic structure, surface chemistry, or defect landscape of the nanocrystals.

This interpretation is consistent with the work of Chiba et al. [15], where $NdCl_3$-treated $CsPbBr_3$ nanocrystals exhibited blue emission and enhanced PLQY, while XPS

depth-profile analysis suggested that Nd was probably located near the nanocrystal surface. Thus, in the present system, Nd should be considered as a possible modifier of the surface or near-surface defect structure rather than as a definitively proven bulk B-site dopant. A key point of interpretation is that the presently available data do not allow the exact structural role of Nd to be determined unambiguously. Neither FE-SEM nor EDX mapping can identify whether Nd occupies B-site lattice positions, is preferentially located at or near the surface, or forms highly dispersed secondary species below the resolution of the employed methods.

This limitation is particularly important for the present high nominal Nd content, because the solid-solubility limit for Nd in the perovskite B-site cannot be established from the current dataset. For the same reason, the proposed mechanism should be regarded as a physically plausible interpretation consistent with the optical observations, not as definitive structural proof. Further clarification would require methods such as high-resolution powder X-ray diffraction with detailed refinement, high-resolution transmission electron microscopy, X-ray photoelectron spectroscopy, or X-ray absorption techniques.

Another limitation is the absence of a directly comparable undoped or differently doped control synthesized and characterized under exactly the same large-scale protocol. Without such a control, it is impossible to rigorously separate the contribution of Nd from the contributions of chloride content, particle size, purification history, and post-synthetic surface treatment. Nevertheless, the dataset does support the following empirical statement: the product obtained from a precursor mixture corresponding to the nominal composition $CsPb(Nd)Br_{3-\gamma}Cl_{\gamma}$ exhibits reproducible blue emission near 458 nm, moderate PLQY for a blue-emitting Nd-containing mixed-halide colloidal system, stable excitation-independent spectral behavior, and nanoscale colloidal stability. This combination of properties is already valuable from an application-oriented point of view.

From a defect-chemistry perspective, the present results are compatible with a scenario in which chloride widens the optical gap while surface passivation suppresses trap-mediated recombination sufficiently to preserve PLQY. Nd may then act either through partial lattice incorporation or through modification of the local chemical environment of the nanocrystal surface and near-surface region. These two possibilities are not mutually exclusive, and both deserve targeted investigation in future work.

Table 1 compares the present material with representative recent examples of blue-emitting perovskite nanomaterials reported in 2022–2024. Several conclusions can be drawn from this comparison. First, the moderate PLQY values in the blue spectral range are generally achieved in highly engineered systems such as nanoplatelets with sophisticated zwitterionic passivation or specially templated composite architectures [10–15]. Second, ultrasmall quantum dots can access even shorter wavelengths, but at the cost of more demanding synthetic control and often more delicate colloidal behavior. Third, Nd-related doping strategies reported in the literature frequently emphasize stabilization or relative PL enhancement compared with a control rather than absolute record PLQY values. Against this background, the performance of the present $CsPb(Nd)Br_{3-\gamma}Cl_{\gamma}$ dispersion should be understood as balanced rather than record-setting: it combines emission near 458 nm, PLQY near 56%, short monoexponential lifetime, and stable colloidal dispersion.

Thus, the obtained results indicate that the sample synthesized with a nominal precursor composition corresponding to 20% neodymium exhibits blue emission with a moderate photoluminescence quantum yield, whereas the nature of neodymium incorporation requires further specialized investigation.

While systems such as ultrasmall QDs and nanoplatelets may deliver higher PLQY or narrower full width at half maximum, they can be more difficult to reproduce on a large scale and may be less convenient for integration into liquid matrices or hybrid

luminescent media. The present synthesis therefore occupies a useful middle ground between optical performance and synthetic practicality. This balance may be relevant for solution-processable photonic layers, wavelength-shifting formulations, and exploratory studies of luminescent liquid systems where absolute record PLQY is not the only criterion. In this sense, the main contribution of the present study is not only the specific value of the emission maximum but the demonstration that a high-nominal-Nd, mixed-halide composition can still provide a coherent and application-relevant optical profile after post-synthetic surface treatment.

Table 1. Comparison of synthesized QDs with modern blue-emitting perovskite nanomaterials.

System/Strategy	Emission Maximum λ_{em} (nm)	PLQY (%)	FWHM (nm)	Lifetime τ, (ns)	Stability/Features	Source (Year)
$CsPb(Nd)Br_{3-\gamma}Cl_{\gamma}$ (this study)	≈458	≈56	—	6.7 ± 0.97	stable peak vs. λexc; nominal composition	This study (2026)
$CsPbBr_3$ QDs (ultra-small, strong quantum confinement)	420–452	≈60	narrow	≈10	increased stability	Otero-Martínez et al., 2024 [9]
$CsPbBr_3$ NPLs ($SnBr_2$-mediated solvothermal)	blue (≈450–470)	—	narrow	—	high color purity	Xu et al., 2023 [10]
$CsPbBr_3$ NPLs (zwitterionic passivation)	≈461	~100	narrow	—	zwitterionic passivation; improved moisture and thermal stability	Liang et al., 2024 [11]
$CsPbBr_3$:xNd^{3+} (optimum ~6% Nd)	green → blue	+20% vs. control	—	≈23	Improved stability	Dongre et al., 2023 [12]
$CsPbBr_3$ (DPSI + silica templates)	green	≈93	narrow	—	high long-term	Wang et al., 2024 [13]
Al-doped $CsPbBr_3$ (RT-synthesis)	≈465	≈65.7	narrow	—	—	Zeng et al., 2022 [14]
$NdCl_3$-treated $CsPbBr_3$ NCs	478	97 in solution; 55 in film	≈15	10.6 in film at 300 K	XPS-confirmed Nd and Cl signals; enhanced PLQY; blue LEDs with EQE 2.7%	Chiba et al., 2020 [15]

Future work should therefore proceed along two complementary directions. The first is mechanistic: a systematic series of $CsPbBr_{3-\gamma}Cl_{\gamma}$ quantum dots prepared with different nominal Nd precursor concentrations and chloride fractions would make it possible to decouple the contributions of Nd-containing species and chloride incorporation to the emission wavelength, PLQY, and decay time.

The second is application-oriented: the present colloid should be tested for photostability, storage stability, and compatibility with selected organic host media. Such experiments would clarify whether the observed optical advantages are retained under realistic device or scintillation conditions.

Table 1 presents a comparison of the synthesized $CsPb(Nd)Br_{3-\gamma}Cl_{\gamma}$ quantum dots with recent representative examples of advances in blue-emitting perovskite nanoparticles.

4. Conclusions

A colloidal method has been developed for the synthesis of Nd-containing mixed-halide perovskite quantum dots, denoted here as $CsPb(Nd)Br_{3-\gamma}Cl_{\gamma}$. This notation is used instead of $CsPb_{1-x}Nd_xBr_{3-\gamma}Cl_{\gamma}$ in order to avoid implying unproven substitutional incorporation of Nd^{3+} at the Pb^{2+} B-site. The obtained samples exhibit blue emission with a maximum at approximately 458 nm, a photoluminescence quantum yield of about 56%, a stable emission peak position upon excitation in the 300–390 nm range, and monoexponential photoluminescence decay with a characteristic lifetime of approximately 6.7 ns. FE-SEM/morphometry and DLS data indicate a nanometer size range and a relatively narrow particle size distribution, while EDX mapping confirms the presence and spatial association of Cs, Pb, Br, Cl, and Nd in the studied material.

The observed blue shift is attributed primarily to chloride incorporation and nanoscale effects, while Nd-containing species may additionally influence the surface or near-surface defect structure. However, the exact chemical and crystallographic state of Nd remains unresolved and requires further XRD, XPS, HR-TEM, or X-ray absorption studies.

In comparison with representative recent blue-emitting perovskite nanomaterials, the studied system is of interest as a colloidal luminescent material combining blue emission, moderate PLQY, and stability in an organic medium. Potential scintillation-related applications remain exploratory and require further radioluminescence, radiation hardness, and host-compatibility testing.

Author Contributions: Conceptualization, Y.K.A.; methodology, A.A.K. and N.E.P.; validation, V.N.K.; formal analysis, V.N.K.; investigation, A.M.P.; resources, V.N.K.; data curation, A.M.P., A.A.K. and N.E.P.; writing—original draft preparation, N.Y.K.; visualization, A.M.P.; supervision, Y.K.A. All authors have read and agreed to the published version of the manuscript.

Funding: The study was supported by the Russian Science Foundation (project No. 25-12-00322).

Institutional Review Board Statement: Not applicable.

Data Availability Statement: The data supporting the findings of this study are contained within the article. Raw microscopy datasets, including the FE-SEM images used for morphometric analysis and elemental mapping, can be provided by the authors upon reasonable request for editorial evaluation and archiving purposes.

Conflicts of Interest: The authors declare no conflicts of interest.

References

1. Babeker, H.; Yang, Y.; Cao, E.; Haider, A.A.; Khan, I.; Qiu, J.; Zhou, D.; Mohammod, O. Ultrastability and Color-tunability of CsPbI3 Nanocrystals Glass Via Doping CoBr2 and Application in WLED. *Ceram. Int.* **2024**, *50*, 24054–24062. [CrossRef]
2. Babeker, H.; Yang, Y.; Qiu, J.; Cao, E.; Haider, A.A.; Liu, Y.; Khan, I.; Zhou, D.; Mohammod, O.; Han, J. Preparation and photoluminescence properties of perovskite $Cs_4PbBr_6/CsPbBr_3$ quantum dots integrated into lithium-borosilicate glass. *Ceram. Int.* **2023**, *49*, 24824–24830. [CrossRef]
3. Zhou, Y.; Chen, J.; Bakr, O.M.; Sun, H.-T. Metal-Doped Lead Halide Perovskites: Synthesis, Properties, and Optoelectronic Applications. *Chem. Mater.* **2018**, *30*, 6589–6613. [CrossRef]
4. Zhang, Y.; Sun, R.; Ou, X.; Fu, K.; Chen, Q.; Ding, Y.; Xu, L.-J.; Liu, L.; Han, Y.; Malko, A.V.; et al. Metal Halide Perovskite Nanosheet for X-ray High-Resolution Scintillation Imaging Screens. *ACS Nano* **2019**, *13*, 2520–2525. [CrossRef] [PubMed]
5. Altudov, Y.K.; Karmokov, A.M.; Pshukov, A.M. Photoluminescent Properties of Aqueous Solutions of Triglycine Sulfate of Various Concentrations. *Pisma Zhurnal Tekhnicheskoi Fiz.* **2025**, *51*, 41–44. [CrossRef]
6. Duan, W.; Hu, L.; Zhao, W.; Zhang, X. Rare-earth ion-doped perovskite quantum dots: Synthesis and optoelectronic properties. *J. Mater. Sci. Mater. Electron.* **2022**, *33*, 19019–19025. [CrossRef]
7. Zhou, L.; Liao, J.-F.; Kuang, D.-B. An Overview for Zero-Dimensional Broadband Emissive Metal-Halide Single Crystals. *Adv. Opt. Mater.* **2021**, *9*, 2100544. [CrossRef]
8. Bizyaeva, A.A.; Stepanova, U.A.; Koroleva, T.V.; Telminov, E.N.; Muradova, A.G. Rare-Earth-Doped Perovskite Nanocrystals: Synthesis and Luminescent Properties. *Adv. Chem. Chem. Technol.* **2022**, *36*, 105–107.

9. Otero-Martínez, C.; Zaffalon, M.L.; Ivanov, Y.P.; Livakas, N.; Goldoni, L.; Divitini, G.; Bora, S.; Saleh, G.; Meinardi, F.; Fratelli, A.; et al. Ultrasmall CsPbBr3 Blue Emis-sive Perovskite Quantum Dots Using K-Alloyed Cs4PbBr6 Nanocrystals as Precursors. *ACS Energy Lett.* **2024**, *9*, 2367–2377. [CrossRef] [PubMed]
10. Xu, Y.; Yu, M.; Li, Y.; Deng, T.; Feng, Y.; Huang, Y.; Yu, C.; Tang, C.; Lin, J. Controllable Synthesis of Blue Emitting $CsPbBr_3$ Nanoplates Via a $SnBr_2$ Mediated Solvothermal Method. *J. Lumin.* **2023**, *263*, 120005. [CrossRef]
11. Liang, J.; Hao, H.; Lei, H.; Yang, J.; Guo, Z.; Liu, G.; Zhao, B.; Shen, W. Highly Stable Deep Blue Emitting $CsPbBr_3$ Nanoplatelets Via Zwitterionic Passivation. *Chem. Eng. J.* **2024**, *495*, 153337. [CrossRef]
12. Dongre, S.S.; R., S.; Moyez, S.A.; Geetha, B. In situ neodymium ion doping into perovskite nanocrystals over ex situ. *Mater. Chem. Phys.* **2023**, *307*, 128221. [CrossRef]
13. Wang, P.; Wang, Z.; Zhu, M.; Cai, Q.; Huang, H.; Tang, C.; Zhang, H.; Fan, C.; Dai, X.; He, H.; et al. Highly Efficient and Ultra-Stable CsPbBr3 Composites for LCD Devices and X-ray Imaging. *J. Mater. Chem. C* **2024**, *12*, 3465–3473. [CrossRef]
14. Zeng, F.; Tan, Y.; Hu, W.; Tang, X.; Zhang, X.; Yin, H. A Facile Strategy to Synthesize High Colour Purity Blue Luminescence Aluminium-Doped CsPbBr3 Perovskite Quantum Dots. *J. Lumin.* **2022**, *245*, 118788. [CrossRef]
15. Chiba, T.; Sato, J.; Ishikawa, S.; Takahashi, Y.; Ebe, H.; Sumikoshi, S.; Ohisa, S.; Kido, J. Neodymium Chlo-ride-Doped Perovskite Nanocrystals for Efficient Blue Light-Emitting Devices. *ACS Appl. Mater. Interfaces* **2020**, *12*, 53891–53898. [CrossRef] [PubMed]
16. Pshukov, A.M.; Kokoeva, A.A.; Yakuba, Y.F.; Kashezhev, A.Z. Perovskite Quantum Dots Doped with Neo-dymium Ions: Synthesis and Optical Properties. *Phys. Chem. Asp. Study Clust. Nanostruct. Nanomater.* **2025**, *17*, 742–751. [CrossRef]

Disclaimer/Publisher's Note: The statements, opinions and data contained in all publications are solely those of the individual author(s) and contributor(s) and not of MDPI and/or the editor(s). MDPI and/or the editor(s) disclaim responsibility for any injury to people or property resulting from any ideas, methods, instructions or products referred to in the content.